Journal of Solid State Chemistry **145,** 88–96 (1999)
Article ID jssc.1999.8224, available online at http://www.idealibrary.com on IDEAL®

Electrical and Magnetic Properties of Strontium Substituted Lanthanum Manganate Perovskite Crystals Prepared Using Fused Salt Electrolysis

W. H. McCarroll

Chemistry Department, Rider University, 2083 Lawrenceville Road, Lawrenceville, New Jersey 08648

K. V. Ramanujachary

Department of Chemistry and Physics, Rowan University, Glassboro, New Jersey 08028; and Department of Chemistry, Rutgers, The State University of New Jersey, Piscataway, New Jersey 08854

and

Ian D. Fawcett and M. Greenblatt

Department of Chemistry, Rutgers, The State University of New Jersey, Piscataway, New Jersey 08854

Received October 26, 1998; in revised form February 5, 1999; accepted February 16, 1999

Crystals of Sr-doped perovskite lanthanum manganates, containing 7–34 mole percent Sr have been grown by fused salt electrolysis using Cs_2MoO_4–MoO_3 solvents in stabilized zirconia crucibles. The rhombohedral crystals grow with cubic-like habits typically with facial areas 0.25–4 mm² on edge with the average facial area decreasing with increasing Sr content. All measured crystals with Sr contents between 11.7 and 33.6 mole percent Sr underwent transitions from a paramagnetic-insulator to a ferromagnetic-metallic state with values of T_c and T_{IM} between 325 and >400 K (for T_{IM}), the values increasing with Sr content. A magnetoresistance of approximately 45% at 375 K was observed for a crystal of composition $Sr_{0.336}La_{0.661}Mn_{0.997}O_3$. The anomalously high $T_c = 325$ K for $Sr_{0.117}La_{0.844}Mn_{0.990}O_3$ for a sample of such low Sr content is interpreted in terms of a high vacancy level on the *A* cation site which stabilizes the rhombohedral perovskite structure, which otherwise might have been expected to be orthorhombic type-1. The formation of Sr-doped lanthanum manganate perovskite at the cathode with the orthorhombic type-2 structure is interpreted in terms of an electrostatically assisted air oxidation mechanism. © 1999 Academic Press

INTRODUCTION

Rare earth manganates of the $LnMnO_3$ type (Ln = rare earth), although known for several decades, have received renewed interest because of the discovery of the colossal magnetoresistance (CMR) phenomenon, wherein the electrical resistivity decreases by orders of magnitude upon the application of magnetic field (1–5). The importance of CMR effects in commercial magnetic recording and retrieval technologies has spurred systematic investigations aimed at understanding the mechanism of CMR in manganates which is critical for the development of materials with improved properties. The double-exchange mechanism, originally proposed by Zener (6), seemed to adequately account for the observed CMR phenomenon at least in rare earth manganates doped with mono- or divalent cations. According to this model, the insulating gap of the undoped antiferromagnetic $LaMnO_3$ corresponds to the charge-transfer energy difference between the O (2*p*) and Mn (3*d*) states. Doping $LaMnO_3$ with mono- or divalent cations at the La site results in mixed valency and strong ferromagnetic correlations at the Mn sites. The loss of scattering due to the magnetic order, near and below the Curie temperature, T_c, is responsible for the insulator–metal transition. Scattering losses in the vicinity of T_c are further minimized by the application of a finite magnetic field, leading to an increased conductivity. While this simple model, based on the mixed-valent Mn, has been remarkably successful in explaining the CMR phenomenon of doped perovskite manganates, recent discoveries of CMR effects in the pyrochlore $Tl_2Mn_2O_7$ (7) raised critical questions concerning the role of mixed valency and crystal structure requirements.

Another important aspect concerning the CMR of manganates is that while some experiments have been carried

0022-4596/99 $30.00

out on single crystal specimens, most investigations reported in the literature have used ceramic specimens or thin films casted from polycrystalline materials. The role of grain boundaries (GB) in the CMR effect has been investigated extensively primarily in polycrystalline materials and in epitaxially grown manganate films (5, 8–12). There is a consensus that GB effects are important in the CMR effect. In general GB are deleterious to the magnetoresistance (MR) near T_c but appear to enhance the effect at $T \ll T_c$. The CMR is maximum at the metal–insulator transition in both polycrystalline and single crystal materials but appears to be much sharper and larger in single crystal or thin film samples.

Studies of CMR of well-characterized, high-quality, relatively defect-free single crystals would help to clarify GB issues and any three-dimensional aspect of the phenomenon to polycrystalline and thin film materials, respectively. Previously, rare earth manganate crystals have been grown by the arc-image floating-zone (FZ) method which requires extremely high temperatures ($\sim$2000°C) and specialized apparatus (13,14). In the FZ method, the oxygen content of the crystals is sensitive to the atmosphere in which they are grown. For example, an argon atmosphere is used in the growth of pure and lightly doped $LaMnO_3$, while mixtures of $Ar + O_2$ are required for the growth of $La_{1-x}Sr_xMnO_3$ phases with $0.0 < x < 0.6$ (13). Crystals are often deformed as a result of a phase transition which takes place on cooling from elevated temperatures. Subsequent annealing in oxygen at 1000°C is required to obtain suitable oxygen stoichiometries (14), but this procedure may not fully repair the lattice damage.

Earlier, we reported on the synthesis and properties of crystals of lanthanum manganates with the rhombohedral perovskite structure (15). The crystal growth was accomplished by fused salt electrolysis (FSE), using molten sodium molybdate–molybdenum(VI) oxide solvents at 975–1000°C in air. In this way, we were able to prepare crystals in which La was partially replaced by Na and/or Sr. These crystals had facial areas of 1 to 4 mm^2 which were suitable for most physical property measurements. However, the crystals obtained were also heavily doped with aluminum, which was abstracted from the crucible containing the melt. While this report clearly indicated the utility of the technique, it was evident that other containers and solvents would be necessary if the method of FSE were to be applied to the production of crystals of rare earth manganates whose composition could be controlled by the user. Recently we reported the growth high quality single crystals of rhombohedral $La_{0.936}Mn_{0.980}O_3$ by using Cs_2MoO_4-based solvents and yttria-stabilized zirconia crucibles (16). In this paper we report on the growth, magnetic susceptibility, electrical resistance, and magnetoresistive properties of Sr-doped lanthanum manganate crystals prepared by this method.

EXPERIMENTAL

The crystals were grown using melts obtained from mixtures of cesium molybdate and molybdenum(VI) oxide to which $MnCO_3$, La_2O_3, and $SrMoO_4$ or $SrCO_3$ were added. Cs_2MoO_4 was prepared by the careful addition of a stoichiometric amount of MoO_3 to a cesium carbonate solution, which was then filtered and evaporated to obtain the hydrated, crystalline cesium molybdate, which was rendered anhydrous by drying for 2 days at 160°C. $SrMoO_4$ was also prepared in this laboratory by wet chemical methods and then ignited at 600°C to remove residual moisture. All starting reagents had stated purities of 99.9% or better. Electrolyses were carried out in air at 950–1000°C using Pt electrodes in 20 cc, yttria-stabilized zirconia crucibles purchased from the McDanel Corporation. The time of electrolysis varied from a few hours to several days using currents between 10 and 40 mA. An 8 to 10 turn 0.5 mm diameter spiral about 1 cm long made from 0.37 mm diameter Pt wire attached to a 0.50 mm diameter shank served as the anode. The cathode was a 1 cm^2 Pt foil or a similar spiral. Runs were carried out in air and were terminated by lifting the electrodes from the melt. Products were washed in warm, dilute solutions of potassium carbonate containing a small amount of ethylenediaminetetraacetic acid. In some instances, solid products were also obtained at the cathode which were chemically cleaned in the same fashion described for the anode products or by washing with warm, dilute HCl when it was clear that the materials obtained were not manganate-based and were resistant to this reagent.

Chemical analyses for Na, La, Sr, Y, Mn, Mo, Pt, and Zr were carried with a Baird Atomic Model 2070 inductively coupled plasma emission spectrometer (ICP). Analyses for main constituents were done in triplicate and are considered to be accurate to within 1–2%. Trace elements (i.e., normally less than 0.1% by weight) were done in duplicate and their accuracy is probably no better than 2%. The cesium content of the crystals were determined by atomic absorption spectroscopy. The formal average valence of manganese was established by an iodometric titration employing an amperometric dead-stop end point method (17, 18). Powder X-ray diffraction (PXD) data was obtained using a Rigaku D-Max 2 system (graphite monochromatized Cu$K\alpha$ radiation). Electrical resistivity measurements on selected crystals were made in a four-point probe configuration and magnetic measurements were carried out on batches of randomly oriented crystals using a Quantum Design SQUID magnetometer (MPMS) between 4–400 K. Magnetoresistance was measured at several temperatures and in magnetic fields up to 5 Tesla (T) in the transverse configuration ($H \perp I$).

RESULTS AND DISCUSSION

Table 1 summarizes the conditions of the crystal growth for the Sr doped lanthanum manganates together with the analyzed compositions. The oxidized products grow directly on the anode spiral in the form of an intergrown, highly reflecting mass of black crystals, which have a cubic-like or square-tabular habit. The dimensions of the individual crystallites were typically between 0.5 and 1.5 mm on edge although a few fragments could be found with edges up to 2 mm long. In general, the average crystal size decreased with increasing Sr content.

Although longer times and lower current densities might be expected to produce the largest crystals, we found that some compromises were necessary for two reasons. First, as deposition proceeds the melt becomes depleted of solute ions, which may lead to the formation of other phases or to other electrode reactions. Secondly, soluble oxidized or reduced species are preferentially formed in the melt at low applied voltages and, as a result, little or no deposition of solid product takes place at the electrodes. On the other hand, high applied voltages resulted in significant evolution of oxygen at the anode. Thus we found that electrolysis for 2 to 4 days at applied voltages between 0.85 and 1.0 V resulted in currents between 10 and 20 mA and most likely to produce the best crystals.

We also found that an operating temperature between 975–1000°C appeared to be optimal. Lower temperatures (900–950°C) result in significantly reduced solute solubilities, decreased product yield, or codeposition of Mn_2O_3 (15). Higher temperatures (i.e., 1025–1050°C) result in increased solvent loss by volatilization and increased attack of the crucible by the melt.

The use of yttria-stabilized zirconia crucibles has a definite advantage over the high-density alumina crucibles used in the earlier studies (15) in that partial replacement of Mn by Al is no longer a factor. Some small replacement of La by Y may occur but for the anode products it seems to be of the order of 0.1 to 0.3 atomic % (i.e., 0.03–0.1% by weight) in the perovskite manganates even after several days usage of the same crucible. Significant amounts of Y and Zr are present in the melt as evidenced by the fact that at high MnO solute concentrations $LaMn_2O_5$-like crystals are formed at the anode which contain relatively large amounts of both zirconium and yttrium. However, incorporation of Zr in the perovskite manganates formed at the anode does not seem to be a factor as evidenced by the fact that this element was typically found at levels less than 0.03% by weight and never exceeding 0.04%.

Levels of Mo found were found to be less than 0.03% provided care was taken to wash the lightly ground crystals prior to analysis. However, multiple washings of the lightly ground crystals reduced these values to less than 0.03% in all cases. A side reaction of the electrolysis, which is sometimes observed, is a slow dissolution of the Pt anode and a partial redeposition at the cathode in the form of a metallic sponge. Since this implies the presence of a soluble Pt species in the melt, we also examined several manganate samples for the presence of Pt and found the amount to be insignificant, i.e., typically on the order of 50 to 200 ppm or less. The total Cs content of the crystals, as determined by atomic absorption spectroscopy, was between 50 and 300 ppm indicating that little or no incorporation of Cs has taken place. Indeed, the sample with 300 ppm Cs purposely was not rigorously washed to see what levels of contamination might be present so we can safely conclude that any incorporated Cs is likely to be less than 0.01 percent by weight.

In Tables 1 and 2 we have chosen to report our stoichiometries for metal content to three decimal places. Although this probably is not always justified for La and Mn, it will generally be so for Sr since the accuracy for this element is closer to 1% and its concentration is relatively small. Further, this convention avoids rounding errors in estimating *A* and *B* site vacancy levels which are discussed later.

Table 2 summarizes the unit cell parameters, the cell volume per formula unit, and the average Mn valence for the anode products as determined by iodometric titration of the phases investigated. The PXD patterns of all these phases could be indexed based on a rhombohedral symmetry. However, broadening of certain reflections at high angles for some compositions is often seen. The effect is illustrated in Fig. 1 for the rhombohedral $\bar{2}20$ and 242 reflections near 68 and 68.5° 2θ, respectively. Figure 1a is for a powder sample prepared from a single crystal fragment taken from sample 180-13A of analyzed composition $Sr_{0.147}La_{0.804}Mn_{1.001}O_3$ and shows that both reflections have similar sharpness and line widths. Figure 1b is for a powder prepared from a random collection of crystals of sample 180-13A and shows a slight, incipient broadening of the $\bar{2}20$ reflection as compared to the 242 reflection. Finally, Fig. 1c obtained for a powdered sample of composition $Sr_{0.218}La_{0.768}Mn_{0.996}O_3$ (83-4A) for a collection of crystals shows a further loss of definition of the reflection at 68°, which is still indexable as the rhombohedral $\bar{2}20$ reflection as part of the data set used for the least squares determination of lattice constants.

These effects might be indicative of the presence of a lower symmetry phase such as the well-established orthorhombic type-2 (19). The powder patterns of these two forms would be very similar and virtually impossible to distinguish with conventional X-ray sources. However, the rhombohedral $\bar{2}20$ is one of the more sensitive reflections to such a distortion and would be expected to split into a doublet while the 242 would remain unsplit. The possibility that the secondary phase might be the occasionally reported monoclinic form cannot be ruled out since the behavior of the powder

TABLE 1
Synthesis Conditions and Analyzed Compositions for (La, Sr)MnO_3 Phases Prepared in Yttria Stabilized Zirconia Crucibles Using Cs_2MoO_4-MoO_3 Solvents

Sample ID	Starting molar ratios Cs_2MoO_4 : MoO_3 : La_2O_3 : MnO : $SrMoO_4$	Time (h)	I (mA)	Temp. (°C)	Sr/La	Sr + La/Mn	Analyzed composition or remarks
44-2A	2.11 : 1.00 : 0.31 : 0.54 : —	112	10–15	970	0.0	1.14	$La_{0.936}Mn_{0.982}O_3$[a]
180-2A1	2.11 : 1.00 : 0.31 : 0.46 : 0.27	30	25	970	0.44	1.9	$Sr_{0.066}La_{0.916}Mn_{0.961}O_3$
180-5A	2.15 : 1.00 : 0.24 : 0.66 : 0.37	90	5	975	0.77	1.3	$Sr_{0.104}La_{0.855}Mn_{0.978}O_3$
180-11A1	2.00 : 1.00 : 0.28 : 0.74 : 0.39	87	18	975	0.70	1.3	$Sr_{0.117}La_{0.844}Mn_{0.990}O_3$
180-13A	2.06 : 1.00 : 0.24 : 0.67 : 0.55	96	15	980	1.15	1.0	$Sr_{0.147}La_{0.804}Mn_{1.001}O_3$
83-1A[a]	2.92 : 1.00 : 0.10 : 0.82 : 0.62	5	10	990	3.0	1.0	Perovskite + Hausmanite
83-2A[a]	2.92 : 1.00 : 0.10 : 0.82 : 0.62	18	10	990	3.0	1.0	Perovskite + Hausmanite
83-4A	2.48 : 1.00 : 0.16 : 0.47 : 0.39	75	10	990	1.2	1.5	$Sr_{0.218}La_{0.768}Mn_{0.996}O_3$
83-5A	2.81 : 1.00 : 0.099 : 0.53 : 0.59	63	13	995	3.0	1.5	$Sr_{0.336}La_{0.661}Mn_{0.997}O_3$
83-6A	2.79 : 1.00 : 0.057 : 0.45 : 0.55	90	10	995	4.8	1.5	$Sr_{0.321}La_{0.679}Mn_{0.994}O_3$
83-8A	2.75 : 1.00 : 0.11 : 0.43 : 0.52	70	10	995	2.3	1.4	$Sr_{0.213}La_{0.762}Mn_{1.001}O_3$
83-8C	2.75 : 1.00 : 0.11 : 0.43 : 0.52	70	10	995	2.3	1.4	$Sr_{0.087}La_{0.920}Mn_{1.002}O_3$

[a] from Ref. (16).

patterns would be very similar (14, 20). Thus, Fig. 1a can be taken as evidence that individual crystals are reasonably homogeneous within the limits of measurement, while Figs. 1b and 1c show evidence for the presence of a second phase with a slightly different composition or the onset of a small distortion to an orthorhombic or perhaps monoclinic form.

A composition gradient within the crystal aggregate or inhomogeneities within an individual crystal fragment could possibly occur as a result of changes in the solute concentrations as the electrolysis proceeds or as a function of the position of growth with respect to the air–melt interface, which might affect total oxygen content. This might also result in a mixture of two hexagonal phases of slightly different composition, but this should cause a broadening of a number of other lines, which we in general have not seen in this system (21). In any event the compositional changes would be expected to be small and any differences in the chemical analysis of individual crystal fragments and a representative bulk sample would probably be within the limits of experimental error of the ICP technique. The level of homogeneity of individual crystals might best be answered by resonance Raman or ferromagnetic resonance spectroscopies, techniques which are not available in our laboratory.

Multiphase effects have also been observed in Sr-doped $LaMnO_3$ crystals grown by the FZ technique. In annealed crystals of analyzed composition $La_{0.86}Sr_{0.15}Mn_{0.95}O_3$,

TABLE 2
Unit Cell Data, Analyzed Average Mn Valences T_c and T_{IM} Values for Rare Earth Manganates Prepared in Yttria Stabilized Zirconia Crucibles Using Cs_2MoO_4–MoO_3 Solvents

Sample ID	Analyzed composition	a, Å	α^0	V_F, Å^3	Mn val	T_c, (T_{IM}), K
44-2A-1	$La_{0.936}Mn_{0.982}MnO_3$	5.4816(4)	60.66(1)	59.10(1)	3.25	230 (240)
180-2A1	$Sr_{0.066}La_{0.916}Mn_{0.961}O_3$	5.4790(3)	60.64(1)	59.00(1)	3.25	290
180-5A	$Sr_{0.104}La_{0.855}Mn_{0.978}O_3$	5.4737(2)	60.54(1)	58.69(1)	3.30	
180-11A	$Sr_{0.117}La_{0.844}Mn_{0.990}O_3$	5.4773(3)	60.57(1)	58.85(1)	3.27	325 (345)
180-13A	$Sr_{0.147}La_{0.804}Mn_{1.001}O_3$	5.4748(3)	60.53(1)	58.711	3.29	
83-8A	$Sr_{0.213}La_{0.762}Mn_{1.001}O_3$	5.4774(3)	60.533(7)	58.80(1)	3.25	365 (370)
83-4A	$Sr_{0.218}La_{0.768}Mn_{0.996}O_3$	5.4784(5)	60.54(1)	58.83(2)	3.27	
83-5A	$Sr_{0.336}La_{0.661}Mn_{0.997}O_3$	5.4702(6)	60.40(1)	58.40(2)	3.36	370 (>400)
83-6A	$Sr_{0.321}La_{0.679}Mn_{0.994}O_3$	5.4712(4)	60.40(1)	58.42(2)	3.34	
83-8C	$Sr_{0.087}La_{0.920}Mn_{1.002}O_3$[a]	$a = 5.545(2)$ $b = 7.774(3)$ $c = 5.546(2)$		59.77(4)	3.06	220

[a] Orthorhombic type-2.

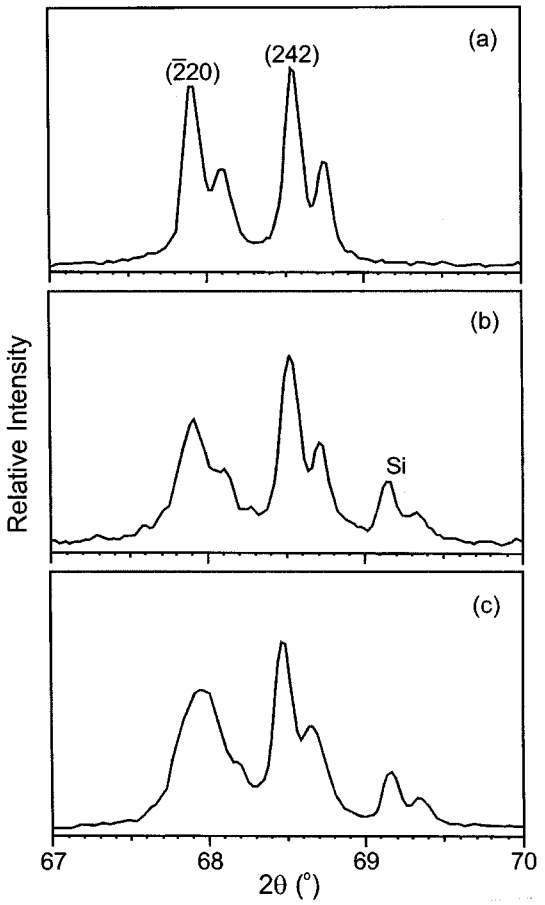

FIG. 1. X-ray powder diffraction patterns of three different Sr substituted lanthanum perovskite manganate samples in the 67–70° 2θ region (Cu$K\alpha$ radiation). Peaks near 69° correspond to the $\alpha1\alpha2$ doublet of internal standard Si. (a) Sample 180-13A, $Sr_{0.147}La_{0.804}Mn_{1.001}O_3$; a sample taken from one ground crystal. (b) 180-13A, a representative sample of several ground crystals. (c) A representative sample of ground crystals of 83-4A, $Sr_{0.218}La_{0.768}Mn_{0.996}O_3$.

a mixture of rhombohedral and orthorhombic forms are observed (22). Vasiliu-Doloc *et al.* have also observed that a crystal having the nominal composition $La_{0.85}Sr_{0.15}MnO_3$, which is orthorhombic type-2 at room temperature transforms to the rhombohedral structure when heated to 360 K (22). They also state that the "hysteretic character" suggests a first-order transition. Thus, the presence of multiphase products at lower temperatures might well be expected. In this respect composition dependent phase transitions have been observed for $Sr_xLa_{1-x}MnO_3$ where the transition temperature decreases from 370 K for $x = 0.15$ to approximately 100 K for $x = 0.20$ (13, 24). Multiphase products have also been observed for polycrystalline specimens of the same system but for $x = 0$–0.075. (25).

The values of V_F, the volume per formula unit, of the Sr-doped manganates are, in general, smaller than that of $La_{0.936}Mn_{0.982}O_3$ reported earlier (16). However, this variation cannot be explained in terms of the ionic size of the dopants or the average formal valence at the Mn site alone, since the process is complicated by the different vacancy levels on both the La and Mn sites.

In general the vacancy levels on both the *A* and *B* (Mn) cation sites tend to decrease as the Sr content increases. By the time the Sr level has reached 12 mole% the Mn site is close to full stoichiometry while a vacancy level of about 4% exists on the *A* sites. We also note that the average Mn valency is more or less constant and independent of Sr content at 3.27 ± 0.02 valence units for samples containing 22 mole% Sr or less. However, the valence has become commensurate with Sr content when the 32–34 mole% Sr level has been reached and essentially full stoichiometry is achieved on both the *A* and *B* sites.

Electrical and Magnetic Properties

The temperature dependent magnetic susceptibilities of several representative samples spanning the range from 0 to 34 mole% Sr are shown in Fig. 2. For the Sr-doped samples a transition to a ferromagnetic state is observed in the temperature range 290–370 K. Clearly, the T_c's observed in this study do not correlate with the average formal valence of Mn, but rather appear to depend on the extent of Sr doping at the La site and the vacancy level on the Mn sites. What is striking about these crystals is that the transition to the ferromagnetic state is particularly sharp for $Sr_{0.336}La_{0.661}Mn_{0.997}O_3$ (83-5A) (Fig. 2) and 85-6A (not shown), both with Sr contents near 33 mole%, less so for sample 83-8A ($Sr_{0.213}La_{0.762}Mn_{1.001}O_3$) and quite broad for

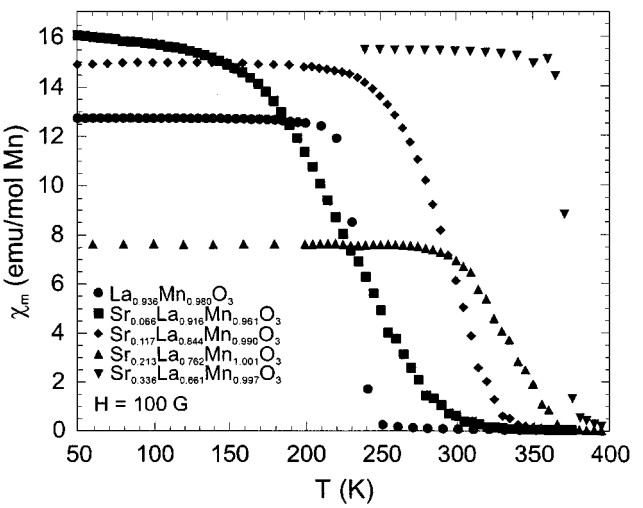

FIG. 2. Variation of the magnetic susceptibility, χ, as a function of temperature for $La_{0.936}Mn_{0.980}O_3$, $Sr_{0.066}La_{0.916}Mn_{0.961}O_3$ (180-2A), $Sr_{0.117}La_{0.844}Mn_{0.990}O_3$ (180-11A1), $Sr_{0.213}La_{0.762}Mn_{1.001}O_3$ (83-8A), and $Sr_{0.336}La_{0.661}Mn_{0.997}O_3$ (83-5A).

180-2A, $Sr_{0.066}La_{0.916}Mn_{0.961}O_3$ which has the lowest Sr content of the doped samples. (Fig. 2) This trend also follows the decreasing level of vacancies on both *A* and *B* sites.

The electrical resistivities of representative crystals as a function of both the temperature and the magnetic field are shown in Figs. 3a–3c. The maximum applied field in all cases is 5 T, the upper limit of our experimental set-up. As expected, the doped manganate crystals showed: (i) an insulator-to-metal transition (T_{IM}) in the vicinity of the ferromagnetic Curie temperature and (ii) a resistivity decrease upon the application of a finite magnetic field. The resistivity at T_{IM} decreases by a factor of nearly 20 as the Sr content increases from 12 to 34 mole% and is consistent with trends observed previously by other workers (13, 26–29). However, the T_{IM} near 345 K for $Sr_{0.117}La_{0.844}Mn_{0.990}O_3$ is unexpected for a sample of such low Sr content (Fig. 3a). Typically samples with 10–12 mole% Sr have either the rhombohedral or orthorhombic type-2 structure and have T_c's 50 to 100 K lower (13, 26–29). This point will be discussed in more detail later.

The term magnetoresistance used here is defined as $100[(\rho_0 - \rho_H)/\rho_0]$, where ρ_H and ρ_0 are the resistivities at applied fields of H and zero Tesla, respectively. At 5 T 35% MR was observed at 325 K for $Sr_{0.117}La_{0.884}Mn_{0.990}O_3$ (Fig. 3a) and 37% MR at 330 K for $Sr_{0.213}La_{0.762}Mn_{1.001}O_3$ (Fig. 3b). The transition to the metallic state in $Sr_{0.336}La_{0.661}Mn_{0.997}O_3$ is above 400 K, the highest temperature of our equipment; a maximum in the MR is found at about 45% at 375 K (Fig. 3c). An interesting feature of Fig. 3c is the relatively high $>25\%$ MR values observed between 250 and 300 K. We have no good explanation for this effect although it may be associated with the lack of grain boundaries and a higher level of crystal perfection than might be found in single crystal material prepared by the FZ method. In this respect, we must point out again that the presence of intergrowths of slightly different composition and/or crystal symmetry within the measured crystal fragments cannot be ruled out. This question is now being addressed at other laboratories using specimens supplied by us.

It is interesting that the self-doped sample $La_{0.936}Mn_{0.982}O_3$ shows a significantly higher MR (ca. 75%) at 5 T and 250 K (16) than any of the above samples. Although a correlation between T_c and the levels of vacancies on the Mn sites has been indicated from studies of K-doped samples (30), the room temperature resistivity of the self-doped sample (ca. 10^{-1} Ω-cm) and those of the Sr-doped samples differ by two-to-three orders of magnitude and do not scale with the formal valence of Mn or the unit cell volume (Table 2). Thus the large variations seen in the transport properties would appear to be related to the defect chemistry such as local disorder with respect to Sr^{2+}/La^{3+} on the *A* site and cation deficiencies on both the *A* and *B* sites of the perovskite structure. It is clear that optimization of the MR properties requires a detailed understanding of how the various defects affect the physical properties. Thus, well-characterized single crystal studies of defects are important in this context.

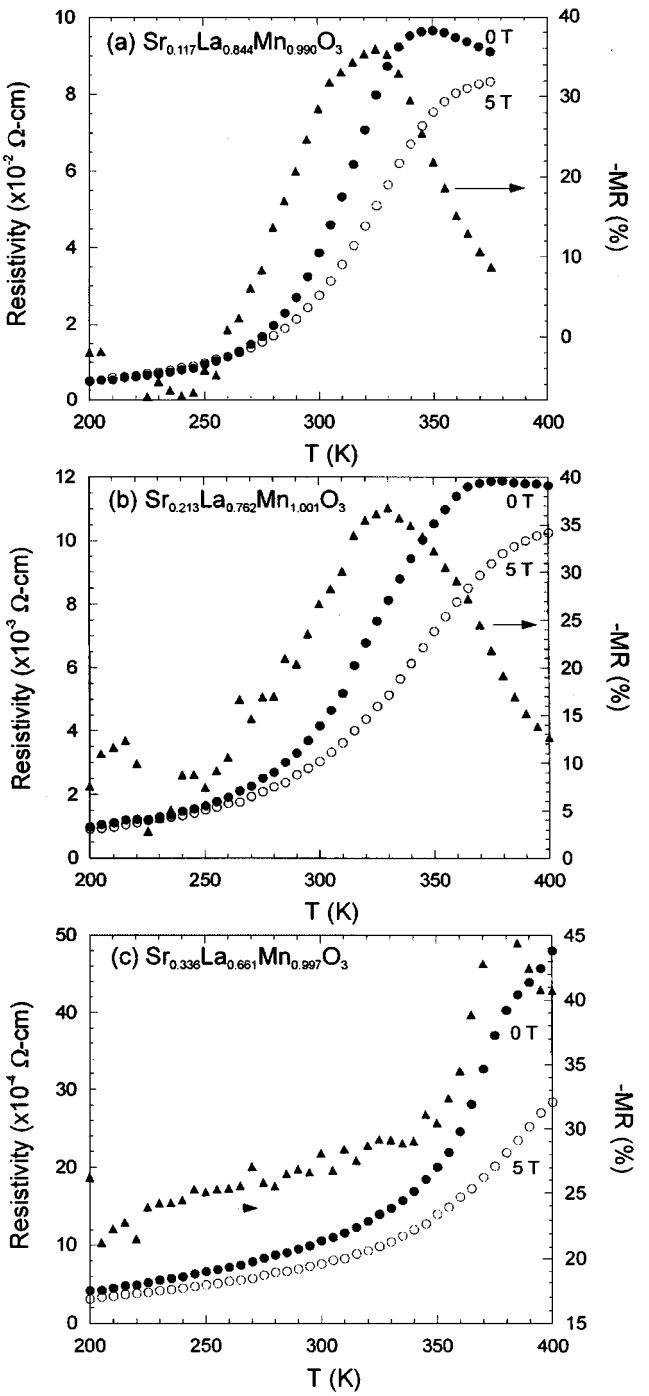

FIG. 3. Variation of the %MR as a function of temperature, and variation of the electrical resistivity as a function of temperature and applied magnetic field for (a) sample 180-11A, $Sr_{0.117}La_{0.844}Mn_{0.990}O_3$, (b) sample 83-8A, $Sr_{0.213}La_{0.762}Mn_{1.001}O_3$, and (c) sample 83-5A, $Sr_{0.336}La_{0.661}Mn_{0.997}O_3$.

Comparison of our results for the Sr-doped lanthanum manganate with those of previous studies is difficult since samples of nominal composition $Sr_xLa_{1-x}MnO_3$ reported in the literature clearly have different levels of cation deficiencies based upon both chemical analyses and unit cell sizes (3, 5, 13, 14, 25, 26–28, 31–33) This is also reflected in the often different temperature dependencies of their magnetic and conductivity properties regardless of whether the samples measured are single crystals, oriented thin films, or polycrystalline ceramics.

However, some comparisons with other bulk single crystal materials appears to be in order. For instance, a single crystal grown by Urushibara *et al.* (13) using the FZ method, which has an analyzed composition of close to $Sr_{0.20}La_{0.80}MnO_3$, displays an MR of about 45% at 325 K ($H = 5$ T, $T_c = 369$ K, $T_{IM} = 360$ K) which compares with our samples of composition $Sr_{0.213}La_{0.762}Mn_{1.001}O_3$ with MR of 37% at 330 K ($H = 5$ T, $T_c = 365$ K, $T_{IM} = 370$ K) and $Sr_{0.336}La_{0.661}Mn_{0.997}O_3$ with MR of 45% at 375 K ($H = 5$ T, $T_c = 370$ K, T_{IM} not observed below 400 K). On the other hand FZ grown crystals studied by Anane *et al.* (26) show MR values between 80 and 90%, albeit well below room temperature, for $x = 0.10$–0.175 in $Sr_xLa_{1-x}MnO_3$, but this ratio drops to about 30% for $x = 0.25$ ($H = 5$ T). Unfortunately no unit cell data are available for these samples. Yang *et al.* prepared polycrystalline $La_{0.83}Sr_{0.17}MnO_3$ by chemie douce techniques and found a 40% MR at 300 K in 5 T (34). Ju and co-workers (4) have reported that epitaxially grown thin films with the composition $Sr_{0.33}La_{0.67}MnO_3$ have MR values of 35% at 330 K near the Curie temperature. However, the IM transitions of the films are much broader than that of the target material from which the films were prepared, suggesting that the films may not be homogeneous. Wilson *et al.* have studied the effect of radiation-induced defects on the MR in deoxygenated $Sr_{0.3}La_{0.7}MnO_3$ films (35). They concluded that strutural defects decrease carrier mobility and impede the ability of an external magnetic field to lower the resistivity.

It has been observed that yttrium substitution in $La_{1-x}A_xMnO_3$ phases (A = Ca, Sr) decreases T_c and enhances MR (36–40). This has been ascribed to an internal pressure effect as a result of a decreased average radius of the A cation, which results in a distortion of the MnO_6 octahedra and a narrowing of the e_g bandwidth. The increase in MR is the result of a lowered hole mobility and an increased coupling between localized and itinerant electrons (41). Although Y appears to be present in our phases, the amounts present, ≤ 0.5 atom% in all cases, are far too low to explain the effects observed here.

Cathode Products

Although our main efforts have focused on the characterization of the products obtained at the anode, some comments about the solid products obtained at the cathode are also in order. In general, two types of product were observed. (1) Normal products which grew on the cathode plate or spiral. They were generally small in yield and were either La rich $(La,Sr)Mo_5O_8$ crystals or a phase whose X-ray diffraction pattern appears to be related to that of $La_5Mo_{32}O_{54}$ (42). (2) A product, which is found above the melt on the cathode shank, which we will refer to as the cathode creep or shank product. This material consists largely of a colorless, or nearly colorless, oxidized matrix containing small, dendritic-like black crystals, which are shown by X-ray powder diffraction to be orthorhombic perovskite phases (see Sample 83-8C in Tables 1 and 2 for an example). These products can be freed of matrix by the wash procedures described previously. Yields are small, rarely exceeding 75–150 mg, although the increasing presence of Sr in the melts seems to increase the total amount of creep product. The crystals are extremely small and ill formed but with an occasional rectangular tablet 0.1–0.2 mm on edge being observed.

While we have not investigated these products extensively, Sample 83-8C appears to be typical of the cathode products, which are only weakly magnetic at room temperature. The cathode products are often contaminated with Pt sponge or yttria-stabilized zirconia crystals. However, sample 83-8C was remarkably free of these contaminants and a chemical analysis was deemed feasible, which yielded a chemical formula of $Sr_{0.087}La_{0.920}Mn_{1.002}0_3$. Its low Mn average valence of 3.06 and orthorhombic structure are reflected in a rather broad, ill-defined transition with a T_c of 220 K as shown in Fig. 4. Because of the small size and poor crystal quality of this sample we were unable to confirm its expected insulating nature. The apparent lack of A or Mn site vacancies is also noteworthy.

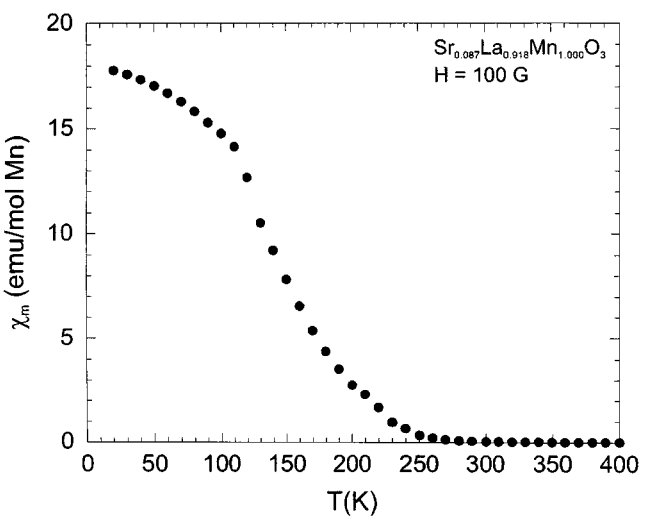

FIG. 4. Variation of the magnetic susceptibility, χ, as a function of temperature for sample 83-8C, $Sr_{0.087}La_{0.918}Mn_{1.000}O_3$.

SUMMARY AND CONCLUSIONS

The relatively simple method of fused salt electrolysis has been used to produce crystals of strontium substituted lanthanum perovskite manganates containing 6 to 34 atom percent Sr at 975–1000°C. These crystals, which grow at the anode, typically have facial areas varying from 0.25 to 4 mm^2. Although longer times of electrolysis tend to produce larger crystals, the composition of the molybdate solvent and the relative concentrations of solute are also important.

Samples with approximately 12 to 34 mole% strontium were found to be ferromagnetic metals with a T_c between 325 and 370 K, the values increasing with increasing Sr content of the crystals. A sample of composition $Sr_{0.336}La_{0.661}Mn_{0.997}O_3$ showed an MR value in excess of 45% at 375 K, but significant MR (>25%) remaining down to 250 K. A crystal of composition $Sr_{0.117}La_{0.844}Mn_{0.990}O_3$ had a T_c of about 325 K, considerably higher than that reported previously for materials with similar Sr contents. This result can be interpreted in terms of a relatively high level of *A* site vacancies resulting in an average Mn valency sufficiently high enough to stabilize the ferromagnetic, metallic, rhombohedral phase where an insulating, paramagnetic, orthorhombic phase might otherwise have been expected.

The formation of perovskite manganate phases at the cathode above the air–melt interface in the form of a cathode creep product is explained on the basis of an electrochemically assisted air oxidation mechanism.

ACKNOWLEDGMENTS

This project was funded in part by NSF- Solid State Chemistry Grant Grant DMR-96-13106. WHM acknowledges with pleasure the assistance of American Chemical Society Project Seed Scholar Susannah Chiu in some of the syntheses and chemical characterization. KVR acknowledges funding from the Research Corporation, Grant CC4366.

REFERENCES

1. K. Chahara, T. Ohno, M. Kasai, and Y. Kozono, *Appl. Phys. Lett*. **63,** 1990 (1993).
2. R. von Helmolt, J. Wocker, B. Holzapfel, M. Schultz, and K. Samwer, *Phys. Rev. Lett*. **71,** 2331 (1993).
3. S. Jin, T. H. Tiefel, M. McCormack, R. A. Fastnacht, R. Ramesh, and L. H. Chen, *Science* **264,** 413 (1994).
4. H. L. Ju, C. Kwon, R. L. Greene, and T. Venkatesan, *Appl. Phys. Lett*. **65,** 2108 (1994).
5. M. McCormack, S. Jin, T. H. Tiefel, R. M. Fleming, and J. M. Phillips, *Appl. Phys. Lett*. **64,** 3045 (1994).
6. C. Zener, *Phys. Rev*. **82,** 403 (1951).
7. M. A. Subramanian, B. H. Toby, A. P. Ramirez, W. J. Marshall, A. W. Sleight, and G. H. Kwei, *Science* **273,** 81 (1996).
8. S. Jin, M. McCormack, T. H. Tiefel, and R. Ramash, *J. Appl. Phys*. **76,** 6929 (1994).
9. A. Gupta, G. O. Gong, G. Xiao, P. R. Duncome, P. Lecoeur, P. Trouilloud, Y. Y. Wang, V. R. Dravid, and J. Z. Sun, *Phys. Rev. B* **54,** R15629 (1996).
10. N. D. Mathur, G. Burnell, S. P. Isaac, T. J. Jackson, B-S. Teo, J. L. MacManus-Driscoll, L. F. Cohen, J. E. Evetts, and M. G. Blamire, *Nature* **387,** 266 (1997).
11. H. Y. Hwang, S.-W. Cheong, N. P. Ong, and B. Batlogg, *Phys. Rev. Lett*. **75,** 2041 (1996).
12. H. L. Ju and H. Sohn, *Solid State Commun*, **102,** 463 (1997).
13. A. Urushibara, Y. Moritomo, T. Arima, A. Asamitsu, G. Kido, and Y. Tokura, *Phys. Rev. B* **51,** 14103 (1995).
14. T. Hasimoto, N. Ishizawa, N. Mizutani, and M. Kato, *J. Cryst. Growth* **84,** 207 (1987).
15. W. H. McCarroll, K. V. Ramanujachary, and M. Greenblatt, *J. Solid State Chem.* **130,** 327 (1997).
16. W. H. McCarroll, K. V. Ramanujachary, and M. Greenblatt, *J. Solid State Chem.* **136,** 322 (1998).
17. F. Licci, G. Turilli, and P. Ferro, *J. Magn. Magn. Mater*. **164,** L268 (1996).
18. G. H. Jeffery, J. Brect, J. Mendham, and R. C. Denrey, "Vogels' Textbook of Quantitative Chemical Analysis," 5th ed., p. 635. Longman/Wiley, New York, 1989.
19. B. C. Hauback, H. Fjellvåg, and N. Sakai, *J. Solid State Chem.* **124,** 43 (1996).
20. A. Maignan, C. Michel, M. Hervieu, and B. Raveau, *Solid State Commun.* **101,** 277 (1997).
21. Recent synchrotron X-ray diffraction studies by D. Cox, V. Golovanov, and L. Mihaly on a powdered sample obtained from a collection of crystals, prepared by fused salt electrolysis, and with the average composition $La_{0.94}Mn_{0.98}O_3$ showed the presence of two hexagonal phases with slightly different cell sizes. Our standard X-ray diffraction unit was not able to make this distinction.
22. L. Vasiliu-Doloc, J. W. Lynn, A. H. Moudden, A. M. de Leon-Guevara, and A. Revcolevschi, *J. Appl. Phys*. **81,** 5491 (1997).
23. M. Itoh, K. Nishi, J. D. Yu, and Y. Inaguma, *Phys. Rev. B* **55,** 14408 (1997).
24. A. Asamitsu, Y. Moritomo, Y. Tomioka, T. Arima, and Y. Tokura, *Nature* **373,** 407 (1995).
25. J. F. Mitchell, D. N. Argyriou, C. D. Potter, D. G. Hinks, J. D. Jorgenson, and S. D. Bader, *Phys. Rev. B* **54,** 6172 (1996).
26. A. Anane, C. Dupas, K. Le Dang, J. P. Renard, P. Veillet, A. M. de Leon Guevara, F. Millot, L. Pinsard, and A. Recolevschi, *J. Phys. Cond. Matt*. **7,** 7015 (1995).
27. H. Kawano, R. Kajimoto, M. Kubota, and H. Yoshizawa, *Phys. Rev. B* **53,** 2202 (1996); *Phys. Rev. B* **53,** R14709 (1996).
28. Y. Tokura, A. Urushibara, Y. Moritomo, T. Arima, A. Asamitsu, G. Kido, and N. Furukawa, *J. Phys. Soc. Japan* **63,** 3931 (1994).
29. R. Mahendiran, S. K. Tiwary, A. K. Raychaudhuri, T. V. Ramakrishnan, R Mahesh, N. Rangavittal, and C. N. R. Rao, *Phys. Rev. B* **53,** 3348 (1996).
30. Y. Ng-Lee, F. Sapiña, E. Martinez-Tamayo, J-V Folgado, R. Ibanez, D. Beltrán, F. Lloret, and A. Segura, *J. Mater. Chem.* **7,** 1905 (1997).
31. G. H. Jonker and J. H. Van Santen, *Physica* **16,** 337 (1950).
32. G. H. Jonker, *Physica* **22,** 707 (1956).
33. I. G. Krogh Anderson, E. Krogh Anderson, P. Norby, and E. Skou, *J. Solid State Chem.* **113,** 320 (1994).
34. S. Yang, C. T. Lin, K. Rogacki, B. Dabrowski, P. M. Adams, and D. M. Speckman, *Chem. Mater*. **10,** 1374 (1998).
35. M. L. Wilson, J. M. Byers, P. C. Dorsey, J. S. Horwitz, D. B. Chrisey, and M. S. Osofsky, *J. Appl. Phys*. **81,** 4971 (1997).
36. S. Jin, H. M. O'Bryan, T. H. Tiefel, M. McCormack, and W. W. Rhodes, *Appl. Phys. Lett*. **66,** 382 (1995).

37. A. Maignan, C. Simon, V. Caignaret, and B. Raveau, *J. Appl. Phys.* **79,** 7891 (1996).
38. M. R. Ibarra, P. A. Algarabel, C. Marquina, J. Blasco, and J. Garcia, *Phys. Rev. Lett.* **75,** 3541 (1995).
39. R. Mahendiran, R. Mahesh, A. K. Raychaudhuri, and C. N. R. Rao, *Phys. Rev. B* **53,** 12160 (1996).
40. C. N. R. Rao and R. Mahesh, *Curr. Opin. Solid State Mater. Sci.* **2,** 32 (1997).
41. J. Fontcuberta, B. Martinez, A. Seffar, S. Pinol, J. L. Garcia-Munoz, and X. Obradors, *Phys. Rev. Lett.* **76,** 1122 (1995).
42. P. Gall, P. Toupet, and P. Gougeon, *Acta Crystallogr C* **49,** 1580 (1993).